

Research

**Cite this article:** Davies B, Herren L. 2022

Robustness of subwavelength devices: a case study of cochlea-inspired rainbow sensors.

Proc. R. Soc. A **478**: 20210765.<https://doi.org/10.1098/rspa.2021.0765>

Received: 1 October 2021

Accepted: 29 April 2022

Subject Areas:

wave motion, applied mathematics

Keywords:

graded metamaterials, hearing, Helmholtz scattering, capacitance matrix, asymptotic expansions, boundary integral methods

Author for correspondence:

Bryn Davies

e-mail: bryn.davies@imperial.ac.uk

One contribution to a special feature 'Asymptotic and numerical models of acoustic, thermal and elastodynamic metamaterials' organised by Sébastien Guenneau, Agnes Maurel and Kim Pham.

Robustness of subwavelength devices: a case study of cochlea-inspired rainbow sensors

Bryn Davies¹ and Laura Herren²¹Department of Mathematics, Imperial College London, 180 Queen's Gate, London SW7 2AZ, UK²Department of Statistics and Data Science, Yale University, New Haven, CT 06511, USA

BD, 0000-0001-8108-2316

We derive asymptotic formulae describing how the properties of subwavelength devices are changed by the introduction of errors and imperfections. As a demonstrative example, we study a class of cochlea-inspired rainbow sensors. These are graded metamaterials which have been designed to mimic the frequency separation performed by the cochlea. The device considered here has similar dimensions to the cochlea and has a resonant spectrum that falls within the range of audible frequencies. We show that the device's properties (including its role as a signal filtering device) are stable with respect to small imperfections in the positions and sizes of the resonators. Additionally, under suitable assumptions, if the number of resonators is sufficiently large, then the device's properties are stable under the removal of a resonator.

1. Introduction

The cochlea is the key organ of mammalian hearing, which filters sounds according to frequency and then converts this information to neural signals. Across the biological world, including in humans, cochleae have remarkable abilities to filter sounds at a very high resolution, over a wide range of volumes and frequencies. This exceptional performance has given rise to a community of researchers seeking to design artificial structures which mimic the function of the cochlea

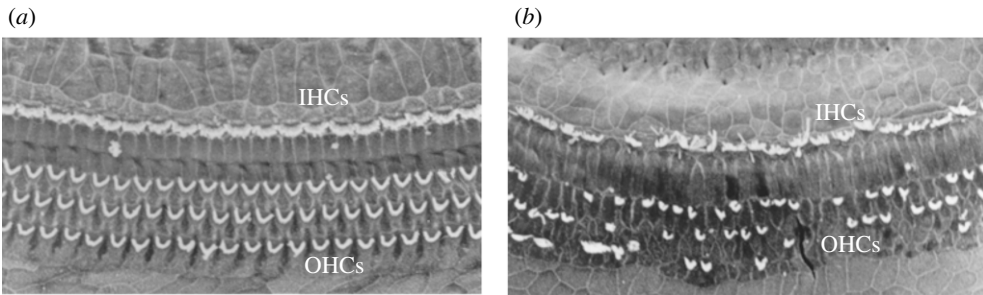


Figure 1. The receptor cells in a (a) normal and (b) damaged cochlea. The receptor cells are arranged as one row of inner hair cells (IHCs) and three rows of outer hair cells (OHCs). In a damaged cochlea, the stereocilia are severely deformed and, in many cases, missing completely. The images are scanning electron micrographs of rat cochlea, provided by Elizabeth M. Keithley.

[1–6]. These devices are based on the phenomenon known as *rainbow trapping*, whereby frequencies are separated in graded resonant media. This has been observed in a range of settings, including acoustics [7], optics [8] (where the term ‘rainbow trapping’ was coined), water waves [9] and plasmonics [10], among others.

The motivation for designing cochlea-inspired sensors is twofold. Firstly, they can be used to design artificial hearing approaches, either through the realization of physical devices [1,11] or by informing computational algorithms [12–14]. Additionally, it is hoped that modelling and building these devices will yield new insight into the function of the cochlea itself. The cochlea’s size and location make experiments on living specimens difficult, meaning that many of the characteristics which are unique to living specimens are still poorly understood. A notable example is the nature of the cochlear amplification mechanism [15]. Artificial cochlea-inspired devices, which can be both modelled and experimented on more easily, provide a convenient platform for theories to be tested in real time and with comparatively minimal expense [1,2,11].

Micro-structured media with strongly dispersive behaviour, such as the cochlea-like rainbow sensors considered here, are examples of *acoustic metamaterials*. Metamaterials are a diverse collection of materials that have extraordinary and ‘unnatural’ properties, such as negative refractive indices and the ability to support cloaking effects [16,17]. One of the challenges in this field, however, is that errors and imperfections are inevitably introduced when devices are manufactured, which has the potential to significantly alter their function. For this reason, a large field has emerged studying *topologically protected* structures, whose properties experience greatly enhanced robustness thanks to the topological properties of the underlying periodic media [18–20]. While the theory of topological protection has deep implications for the design of rainbow sensors [21], there is yet to be a link established with biological structures; we will to study the robustness of a bio-inspired graded metamaterial in this work.

The biological cochlea has a remarkable ability to function effectively even when significantly damaged. As depicted in figure 1, cochlear receptor cells are often significantly damaged in older organisms. However, it has been observed that humans can lose as much as 30–50% of their receptor cells without any perceptible loss of hearing function [22,23] (see figure 1 for an example of receptor cell damage). This remarkable robustness is part of the motivation for this study: how do cochlea-inspired rainbow sensors behave under similar errors and imperfections? The aim of this work is to derive formulae which describe how the properties of a cochlea-inspired rainbow sensor are affected by the introduction of perturbations. This will give quantitative insight into the extent to which these devices are robust with respect to manufacturing errors and may also yield insight into the remarkable robustness of the cochlea itself.

We will study a passive device consisting of an array of material inclusions whose properties resemble those of air bubbles in water. These inclusions act as resonators, oscillating with the

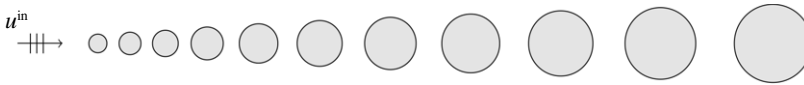


Figure 2. A cochlea-inspired rainbow sensor. The gradient in the sizes of the resonators means the device separates different frequencies in space: higher frequencies will give a peak amplitude to the left of the array, while lower frequencies will give a maximal response further to the right. This mimics the action of the cochlea in filtering sound waves. In this work, we study the system in a low-frequency limit, implying that the wavelength of u^{in} is much larger than the total length of the array.

so-called breathing modes, and exhibit resonance at subwavelength scales, often known as *Minnaert resonance* [24–26]. Devices have been built based on these principles by injecting bubbles into polymer gels [27,28]. It was shown in [4] that by grading the size of the resonators, to give the geometry depicted in figure 2, it is possible to replicate the spatial frequency separation of the cochlea.

We will use boundary integral methods to analyse the scattering of the acoustic field by the cochlea-inspired rainbow sensor [29]. We will define the notion of subwavelength resonance as an asymptotic property, in terms of the material contrast, and perform an asymptotic analysis of the structure’s resonant modes. This first-principles approach yields an approximation in terms of the *generalized capacitance matrix*. We will recap this theory in §2 and refer the reader to Ammari *et al.* [30] for a more thorough exposition. In §3, we study the effect of small perturbations to the size and position of the resonators. The derived formulas show that the rainbow sensor’s properties are stable with respect to these imperfections. Then, in §4, we examine more drastic perturbations, namely those caused by removing resonators from the array. This is inspired by the images in figure 1, where in many places the receptor cell stereocilia have been completely destroyed. We will show that, provided that array is sufficiently large, the sensor’s properties are nonetheless stable. Finally, in §5, we study the equivalent signal transformation that is induced by the cochlea-inspired rainbow sensor and show that its properties are stable with respect to changes in the device.

2. Mathematical preliminaries

(a) Problem setting

We will study a Helmholtz scattering problem to model the scattering of time-harmonic acoustic waves by the resonator array. The resonators are modelled as material inclusions D_1, \dots, D_N which are disjoint, bounded and have boundaries in $C^{1,\alpha}$ for some $0 < \alpha < 1$. We suppose that wave propagation inside the resonators can be modelled by

$$\left(\nabla \cdot \frac{1}{\rho} \nabla + \frac{\omega^2}{\kappa} \right) u = 0, \quad (2.1)$$

where ρ is the density of the material and κ is the bulk modulus. A similar equation is assumed to hold in the background medium, with corresponding parameters ρ_0 and κ_0 . Denoting the wave speeds inside the resonators as $v = \sqrt{\kappa/\rho}$ and in the background medium as $v_0 = \sqrt{\kappa_0/\rho_0}$, we introduce the wavenumbers

$$k = \frac{\omega}{v} \quad \text{and} \quad k_0 = \frac{\omega}{v_0}.$$

Additionally, we introduce the dimensionless contrast parameter

$$\delta = \frac{\rho}{\rho_0}, \quad (2.2)$$

which is the ratio of the densities of the materials inside and outside the resonators. The scattering problem, due to the resonator array $D = D_1 \cup \dots \cup D_N$, is then given by

$$\begin{cases} (\Delta + k_0^2)u = 0 & \text{in } \mathbb{R}^3 \setminus \overline{D}, \\ (\Delta + k^2)u = 0, & \text{in } D, \\ u_+ - u_- = 0, & \text{for } \partial D, \\ \delta \frac{\partial u}{\partial \nu} \Big|_+ - \frac{\partial u}{\partial \nu} \Big|_- = 0, & \text{on } \partial D, \\ u^s := u - u^{\text{in}} \text{ satisfies the SRC,} & \text{as } |x| \rightarrow \infty, \end{cases} \quad (2.3)$$

where SRC refers to the Sommerfeld radiation condition, which guarantees that the scattered waves radiate energy outwards to the far field [29]. Here, the subscript $+$ and $-$ denote limits from outside and inside D , respectively.

Definition 2.1 (Resonance). We define a *resonant frequency* to be $\omega \in \mathbb{C}$ such that there exists a non-zero solution u to (2.3) in the case that $u^{\text{in}} = 0$. The solution u is the *resonant mode* associated with ω .

In this work, we will characterize *subwavelength* resonance in terms of the limit of the contrast parameter δ being small. In particular, we assume that

$$\delta \ll 1 \quad \text{while } v, v_0, \frac{v}{v_0} = O(1) \text{ as } \delta \rightarrow 0. \quad (2.4)$$

One consequence of these assumptions is that $\kappa/\kappa_0 = O(\delta)$. This approach allows us to fix the size and position of the resonators and study subwavelength resonant modes as those which exist at asymptotically low frequencies when δ is small.

Definition 2.2 (Subwavelength resonance). We define a subwavelength resonant frequency to be a resonant frequency $\omega = \omega(\delta)$ that depends continuously on δ and satisfies

$$\omega \rightarrow 0 \quad \text{as } \delta \rightarrow 0.$$

This asymptotic approach has been shown to be effective at modelling devices based on the canonical example of air bubbles in water [26,30], where the contrast parameter is approximately $\delta \approx 10^{-3}$. Furthermore, this asymptotic definition of subwavelength resonance reveals that there is a fundamental difference between these resonant modes and those which are not subwavelength, and leads to the following existence result:

Lemma 2.3. *A system of N subwavelength resonators has N subwavelength resonant frequencies with positive real part, counted up to multiplicity.*

Proof. This follows using Gohberg–Sigal theory to perturb the solutions that exist in the limiting case where $\delta = 0$, $\omega = 0$, see ([30], theorem 2.4) for details, which generalizes the original result proved in ([26], lemma 2.2). ■

The subwavelength resonant frequencies of a cochlea-inspired rainbow sensor composed of 22 subwavelength resonators are shown in figure 3. An array of spherical resonators totalling 35 mm in length and having the material parameters of air bubbles in water is simulated using the multipole expansion method (see §2d for details). The resonators are chosen such that the i th resonator has radius $R_i = as^{i-1}$, where $a = 0.1$ mm and $s = 1.05$. The positioning of the resonators follows a similar exponential distribution, with the distance between the centres of the i th and $i + 1$ st resonators being equal to $2R_i + R_{i+1}$. The real parts of the resonant frequencies span the range 7.4–33.8 kHz (figure 3 shows angular frequency). This range can be finetuned to match the desired function (or to match the range of human hearing more closely) [2]. The negative imaginary parts describe the loss of energy to the far field.

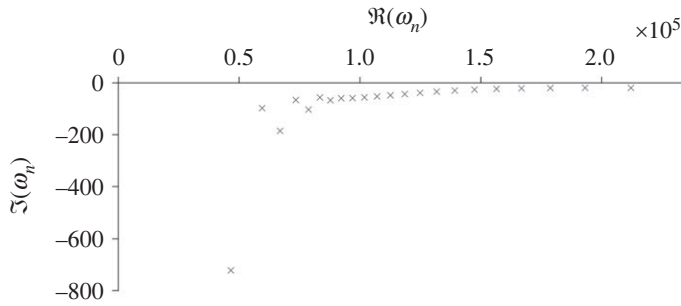


Figure 3. The 22 subwavelength resonant frequencies of a cochlea-inspired rainbow sensor composed of 22 subwavelength resonators, plotted in the lower-right complex plane. This structure measures 35mm long (to match the uncoiled cochlea) and has the material properties of air bubbles in water, giving $\delta = 1.2 \times 10^{-3}$. These simulations are performed on the full differential problem using a multipole expansion.

(b) Boundary integral operators

In order to model the scattering of waves by the array D , we will use layer potentials to represent solutions.

Definition 2.4 (Single layer potential). Given a bounded domain $D \subset \mathbb{R}^3$ and a wavenumber $k \in \mathbb{C}$ we define the Helmholtz single layer potential as

$$\mathcal{S}_D^k[\varphi](x) = \int_{\partial D} G^k(x-y)\varphi(y) \, d\sigma(y), \quad \varphi \in L^2(\partial D), \quad x \in \mathbb{R}^3,$$

where Green's function G is given by

$$G^k(x) = -\frac{e^{ik|x|}}{4\pi|x|}, \quad x \neq 0.$$

The value of the single layer potential is that we can use it to represent solutions to the Helmholtz scattering problem (2.3). In particular, there exist some densities $\psi, \phi \in L^2(\partial D)$ such that

$$u(x) = \begin{cases} u^{\text{in}}(x) + \mathcal{S}_D^{k_0}[\psi](x), & x \in \mathbb{R}^3 \setminus \bar{D}, \\ \mathcal{S}_D^k[\phi](x), & x \in D. \end{cases} \quad (2.5)$$

This representation means that the Helmholtz equations and the radiation condition from (2.3) are necessarily satisfied. It remains only to find densities $\psi, \phi \in L^2(\partial D)$ such that the two transmission conditions across the boundary ∂D are satisfied. See [29] for more details on the use of layer potentials in modelling scattering problems. In this work, we will make use of some elementary properties. Since we define subwavelength resonance as an asymptotic property (definition 2.2), we will make use of the asymptotic expansion

$$\mathcal{S}_D^k = \mathcal{S}_D^0 + k\mathcal{S}_{D,1} + O(k^2), \quad \text{as } k \rightarrow 0, \quad (2.6)$$

where $\mathcal{S}_{D,1}[\varphi] = (4\pi i)^{-1} \int_{\partial D} \varphi \, d\sigma$ and convergence holds in the $L^2(\partial D) \rightarrow L^2(\partial D)$ operator norm. In order to derive leading-order approximations, we will make use of the fact that \mathcal{S}_D^0 is invertible ([29], lemma 2.6):

Lemma 2.5. \mathcal{S}_D^0 is invertible as a map from $L^2(\partial D)$ to $H^1(\partial D)$.

(c) The generalized capacitance matrix

Studying the subwavelength resonant properties of the high-contrast structure as an asymptotic property in terms of $\delta \ll 1$ leads to a concise characterization of the resonant states. In particular,

we find that the leading-order properties of the resonant frequencies and associated eigenmodes are given in terms of the eigenstates of the *generalized capacitance matrix*, as introduced in [30]. This is a generalization of the notion of capacitance that is widely used in electrostatics to model the distributions of potential and charge in a system of conductors [31].

Definition 2.6 (Capacitance matrix). Given $N \in \mathbb{N}$ disjoint inclusions $D_1, \dots, D_N \subset \mathbb{R}^3$, the associated capacitance matrix $C \in \mathbb{R}^{N \times N}$ is defined as

$$C_{ij} = - \int_{\partial D_i} (S_D^0)^{-1} [\chi_{\partial D_j}] d\sigma, \quad i, j = 1, \dots, N,$$

where $\chi_{\partial D_i}$ is the characteristic function of the boundary ∂D_i .

In this work, we are interested in cochlea-like rainbow sensors that have resonators with increasing size. In general, in order to use capacitance coefficients to understand the resonant properties of an array of non-identical resonators, we need to re-scale the coefficients. The *generalized capacitance matrix* that we obtain is studied at length in [30]. With this approach, we can study arrays of resonators with different sizes, shapes and material parameters. In this work, we are assuming the resonators all have the same interior material parameters (given by the wave speed v and contrast parameter δ) so only need to re-scale according to the different sizes of the resonators.

Definition 2.7 (Volume scaling matrix). Given $N \in \mathbb{N}$ disjoint inclusions $D_1, \dots, D_N \subset \mathbb{R}^3$, the volume scaling matrix $V \in \mathbb{R}^{N \times N}$ is the diagonal matrix given by

$$V_{ii} = \frac{1}{\sqrt{|D_i|}}, \quad i = 1, \dots, N,$$

where $|D_i|$ is the volume of D_i .

Definition 2.8 (Generalized capacitance matrix). Given $N \in \mathbb{N}$ disjoint inclusions $D_1, \dots, D_N \subset \mathbb{R}^3$ with identical interior material parameters, the associated (symmetric) generalized capacitance matrix $\mathcal{C} \in \mathbb{R}^{N \times N}$ is defined as

$$\mathcal{C} = VCV.$$

In previous works, the generalized capacitance matrix is typically defined as the asymmetric matrix V^2C (see [30] and references therein). Here, we will want to use some of the many existing results about perturbations of eigenstates of symmetric matrices so opt for the symmetric version. Note that $\mathcal{C} = VCV$ is similar to V^2C . The value of the generalized capacitance matrix is clear from the following results, which were proved in ([32], theorem 2.7).

Theorem 2.9. Consider a system of N subwavelength resonators in \mathbb{R}^3 and let $\{(\lambda_n, \mathbf{v}_n) : n = 1, \dots, N\}$ be the eigenpairs of the (symmetric) generalized capacitance matrix $\mathcal{C} \in \mathbb{R}^{N \times N}$. As $\delta \rightarrow 0$, the subwavelength resonant frequencies satisfy the asymptotic formula

$$\omega_n = \sqrt{\delta v^2 \lambda_n} - i\delta \tau_n + O(\delta^{3/2}), \quad n = 1, \dots, N,$$

where the second-order coefficients τ_n are given by

$$\tau_n = \frac{v^2}{8\pi v_0} \frac{1}{\|\mathbf{v}_n\|^2} \mathbf{v}_n^\top VCV \mathbf{v}_n, \quad n = 1, \dots, N,$$

with J being the $N \times N$ matrix of ones.

Corollary 2.10. Let v_n be the normalized eigenvector of C associated with the eigenvalue λ_n . Then the normalized resonant mode u_n associated with the resonant frequency ω_n is given, as $\delta \rightarrow 0$, by

$$u_n(x) = \begin{cases} v_n^\top V S_D^{k_0}(x) + O(\delta^{1/2}), & x \in \mathbb{R}^3 \setminus \bar{D}, \\ v_n^\top V S_D^k(x) + O(\delta^{1/2}), & x \in D, \end{cases}$$

where $S_D^k : \mathbb{R}^3 \rightarrow \mathbb{C}^N$ is the vector-valued function given by

$$S_D^k(x) = \begin{pmatrix} S_D^k[\psi_1](x) \\ \vdots \\ S_D^k[\psi_N](x) \end{pmatrix}, \quad x \in \mathbb{R}^3 \setminus \partial D,$$

with $\psi_i := (S_D^0)^{-1}[\chi_{\partial D, i}]$.

Remark 2.11. Since C is symmetric, V is diagonal and J is positive semi-definite, it holds that $\tau_n \geq 0$ for all $n = 1, \dots, N$. This corresponds to the loss of energy from the system.

We will shortly want to study how the properties of the generalized capacitance matrix C vary when changes are made to the structure D . For this reason, we will often write $C = C(D)$ to emphasize the dependence of the generalized capacitance matrix on the geometry of D . Similarly, we will write $\lambda_i = \lambda_i(D)$ and $\tau_i = \tau_i(D)$ for the quantities from theorem 2.9. With this in mind, it is important to notice that the asymptotic expansion in theorem 2.9 is uniform with respect to geometric perturbations that keep the resonators separated (this breaks down if they touch or overlap). This is a useful property of this result which has been used in many places, such as in ([33], theorem 2), where the result for ϵ -small resonators is proved as a modification of ([32], theorem 2.7).

(d) Numerical methods

In the subsequent analysis, we will often want to compare asymptotic results with the behaviour of the ‘exact’ problem. These ‘exact’ results are numerical solutions to (2.3), computed using a three-dimensional multipole expansion. This uses the fact that the spherical waves $j_l(kr)Y_l^m(\theta, \phi)$ and $h_l^{(1)}(kr)Y_l^m(\theta, \phi)$ form a basis of the solution space of the radially symmetric Helmholtz equation in the spherical polar coordinate system (r, θ, ϕ) . Here, for $l \in \mathbb{N}$ and $m = -l, \dots, l$, $Y_l^m(\theta, \phi)$ are the spherical harmonics, j_l are the spherical Bessel functions of the first kind and $h_l^{(1)}$ are the spherical Hankel functions of the first kind. Then, if D is a sphere with radius R , we have that

$$S_D^k[Y_l^m](r, \theta, \phi) = \begin{cases} c_{jl}(kR)h_l^{(1)}(kr)Y_l^m(\theta, \phi), & |r| > R, \\ ch_l^{(1)}(kR)j_l(kr)Y_l^m(\theta, \phi), & |r| \leq R, \end{cases} \quad (2.7)$$

where $c = -ikR^2$. We can then use addition formulae to generalize (2.7) to the case of multiple spheres. The resulting representation can be used to give a discrete approximation for solutions to the differential problem (2.3). For more details, see the appendices of [20].

All the numerical experiments in this work are performed using the canonical example of air bubbles in water. That is, $\rho = 1.2 \text{ kg m}^{-3}$, $\kappa = 10^5 \text{ Pa}$, $\rho_0 = 10^3 \text{ kg m}^{-3}$ and $\kappa_0 = 2 \times 10^9 \text{ Pa}$. This gives a value for the dimensionless asymptotic parameter of $\delta = 1.2 \times 10^{-3}$.

3. Imperfections in the device

We will begin by deriving formulas to describe the effects of making small perturbations to the positions and sizes of the resonators, as depicted in figure 4. Perturbations of this nature are important as they will be introduced when a device is manufactured. The results in this section give quantitative estimates on the extent to which the perturbations of the structure’s properties are stable with respect to small imperfections.

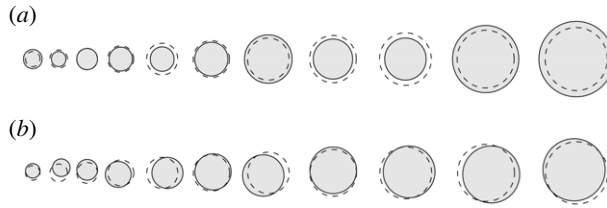


Figure 4. We study the effects of adding random perturbations to the (a) size and (b) position of the resonators in a cochlea-inspired rainbow sensor. The original structure is shown in dashes.

(a) Dilute approximations

In order to simplify the analysis, and to allow us to work with explicit formulae, we will make an assumption that the resonators are small compared with the distance between them. In particular, we will assume that each resonator D_i is given by $B_i + \epsilon^{-1}z_i$ where $B_i \subset \mathbb{R}^3$ is some fixed domain, $z_i \in \mathbb{R}^3$ is some fixed vector and $0 < \epsilon \ll 1$ is some small parameter. We will assume that each fixed domain B_i , for $i = 1, \dots, N$, is positioned so that it contains the origin and that the complete structure is given by

$$D = \bigcup_{i=1}^N D_i, \quad D_i = (B_i + \epsilon^{-1}z_i). \quad (3.1)$$

Under this assumption, the generalized capacitance matrix has an explicit leading-order asymptotic expression in terms of the *dilute* generalized capacitance matrix:

Definition 3.1 (Dilute generalized capacitance matrix). Given $0 < \epsilon \ll 1$ and a resonator array that is ϵ -dilute in the sense of (3.1), the associated dilute generalized capacitance matrix $\mathcal{C}^\epsilon \in \mathbb{R}^{N \times N}$ is defined as

$$\mathcal{C}_{ij}^\epsilon = \begin{cases} \frac{\text{Cap}_{B_i}}{|B_i|}, & i = j, \\ -\epsilon \frac{\text{Cap}_{B_i} \text{Cap}_{B_j}}{4\pi |z_i - z_j| \sqrt{|B_i| |B_j|}}, & i \neq j, \end{cases}$$

where we define the capacitance Cap_B of a set $B \subset \mathbb{R}^3$ to be the strictly positive number given by

$$\text{Cap}_B := - \int_{\partial B} (\mathcal{S}_B^0)^{-1} [\chi_{\partial B}] d\sigma.$$

Lemma 3.2. Consider a resonator array that is ϵ -dilute in the sense of (3.1). In the limit as $\epsilon \rightarrow 0$, the asymptotic behaviour of the (symmetric) generalized capacitance matrix is given by

$$\mathcal{C} = \mathcal{C}^\epsilon + O(\epsilon^2) \quad \text{as } \epsilon \rightarrow 0.$$

Proof. This was proved in ([33], lemma 1) as a modification of the original result in ([20], lemma 4.3). ■

Remark 3.3. It would also be possible to state an appropriate diluteness condition as a rescaling of the sizes of the resonators, by taking $D_i = \epsilon B_i + z_i$ in (3.1). This would give analogous but rescaled results, as used for the analysis in [20].

(b) Changes in size

We first consider imperfections due to changes in the size of the resonators. In particular, suppose there exist some factors $\alpha_1, \dots, \alpha_N$ such that the perturbed structure is given by

$$D^{(\alpha)} = \bigcup_{i=1}^N ((1 + \alpha_i)B_i + \epsilon^{-1}z_i). \quad (3.2)$$

We will assume that the perturbations $\alpha_1, \dots, \alpha_N$ are small in the sense that there exists some parameter α such that $\alpha_i = O(\alpha)$ as $\alpha \rightarrow 0$.

Lemma 3.4. *Suppose that a resonator array D is deformed to give $D^{(\alpha)}$, as defined in (3.2), and that the size change parameters $\alpha_1, \dots, \alpha_N$ satisfy $\alpha_i = O(\alpha)$ as $\alpha \rightarrow 0$ for all $i = 1, \dots, N$. Then, for fixed $0 < \epsilon \ll 1$, the dilute generalized capacitance matrix associated with $D^{(\alpha)}$ is given by*

$$C^\epsilon(D^{(\alpha)}) = C^\epsilon(D) + A(\alpha),$$

where $A(\alpha)$ is a symmetric $N \times N$ -matrix whose Frobenius norm satisfies $\|A\|_F = O(\alpha)$ as $\alpha \rightarrow 0$. Furthermore, the error bound $\|C^\epsilon(D^{(\alpha)}) - C^\epsilon(D)\|_F = O(\alpha)$ as $\alpha \rightarrow 0$ is uniform with respect to $\epsilon \in [0, 1]$.

Proof. Making the substitution $B_i \mapsto (1 + \alpha_i)B_i$ in definition 3.1 gives

$$C_{ij}^\epsilon(D^{(\alpha)}) = \begin{cases} \frac{\text{Cap}_{B_i}}{(1 + \alpha_i)|B_i|}, & i = j, \\ -\epsilon \frac{\text{Cap}_{B_i} \text{Cap}_{B_j}}{4\pi |z_i - z_j| \sqrt{(1 + \alpha_i)(1 + \alpha_j)} \sqrt{|B_i||B_j|}}, & i \neq j. \end{cases}$$

For small α we can expand the denominators to give

$$C_{ij}^\epsilon(D^{(\alpha)}) = \begin{cases} (1 - \alpha_i) \frac{\text{Cap}_{B_i}}{|B_i|} + O(\alpha^2), & i = j, \\ -\epsilon \left[(1 - \frac{1}{2}(\alpha_i + \alpha_j)) \frac{\text{Cap}_{B_i} \text{Cap}_{B_j}}{4\pi |z_i - z_j| \sqrt{|B_i||B_j|}} + O(\alpha^2) \right], & i \neq j, \end{cases}$$

as $\alpha \rightarrow 0$. From this, we can see that

$$A_{ij} = C_{ij}^\epsilon(D^{(\alpha)}) - C_{ij}^\epsilon(D) = \begin{cases} -\alpha_i \frac{\text{Cap}_{B_i}}{|B_i|} + O(\alpha^2), & i = j, \\ \epsilon \left[\frac{1}{2}(\alpha_i + \alpha_j) \frac{\text{Cap}_{B_i} \text{Cap}_{B_j}}{4\pi |z_i - z_j| \sqrt{|B_i||B_j|}} + O(\alpha^2) \right], & i \neq j, \end{cases}$$

as $\alpha \rightarrow 0$. To see that the convergence of $C^\epsilon(D^{(\alpha)})$ to $C^\epsilon(D)$ is uniform in $\epsilon \in [0, 1]$, notice that the diagonal terms of A do not depend on ϵ and the absolute value of the off-diagonal terms is a monotonic function of ϵ . ■

Theorem 3.5. *Suppose that a resonator array D is ϵ -dilute in the sense of (3.1) and is deformed to give $D^{(\alpha)}$, as defined in (3.2), for size change parameters $\alpha_1, \dots, \alpha_N$ which satisfy $\alpha_i = O(\alpha)$ as $\alpha \rightarrow 0$ for all $i = 1, \dots, N$. Then, the resonant frequencies satisfy*

$$|\omega_n(D) - \omega_n(D^{(\alpha)})| = O\left(\sqrt{\delta(\alpha + \epsilon^2)}\right),$$

as $\alpha, \delta, \epsilon \rightarrow 0$.

Proof. From lemma 3.4, we have that $C^\epsilon(D^{(\alpha)}) = C^\epsilon(D) + A(\alpha)$ where A is a symmetric $N \times N$ -matrix. Then, by the Wielandt–Hoffman theorem [34], it holds that the eigenvalues of $C^\epsilon(D)$ and

$\mathcal{C}^\epsilon(D^{(\alpha)})$, which we denote by $\lambda_i^\epsilon(D)$ and $\lambda_i^\epsilon(D^{(\alpha)})$, respectively, satisfy

$$\sum_{n=1}^N (\lambda_n^\epsilon(D) - \lambda_n^\epsilon(D^{(\alpha)}))^2 \leq \|A\|_F^2. \quad (3.3)$$

From this we can see that $|\lambda_i^\epsilon(D) - \lambda_i^\epsilon(D^{(\alpha)})| = O(\alpha)$ as $\alpha \rightarrow 0$, since $\|A\|_F = O(\alpha)$ as $\alpha \rightarrow 0$ by lemma 3.4. Further, this convergence is uniform in ϵ and δ (from lemma 3.4 and since these quantities do not depend on δ). By a similar argument, and using lemma 3.2, we have that

$$|\lambda_n(D) - \lambda_n^\epsilon(D)| = O(\epsilon^2) \quad \text{and} \quad |\lambda_n(D^{(\alpha)}) - \lambda_n^\epsilon(D^{(\alpha)})| = O(\epsilon^2), \quad \text{as } \epsilon \rightarrow 0. \quad (3.4)$$

Again, we have that this convergence is uniform with respect to α and δ , since there is no dependence on either α or δ (crucially, $\lambda_n(D^{(\alpha)}) - \lambda_n^\epsilon(D^{(\alpha)})$ is constant as a function of α). Finally, we use theorem 2.9 to find the resonant frequencies when $\delta \rightarrow 0$:

$$\begin{aligned} |\omega_n(D) - \omega_n(D^{(\alpha)})| &= \left| \sqrt{\delta v^2 \lambda_n(D)} - \sqrt{\delta v^2 \lambda_n(D^{(\alpha)})} \right| + O(\delta) \\ &\leq \sqrt{\delta v^2} \sqrt{|\lambda_n(D) - \lambda_n(D^{(\alpha)})|} + O(\delta). \\ &\leq \sqrt{\delta v^2} \sqrt{|\lambda_n(D) - \lambda_n^\epsilon(D)| + |\lambda_n^\epsilon(D) - \lambda_n^\epsilon(D^{(\alpha)})| + |\lambda_n^\epsilon(D^{(\alpha)}) - \lambda_n(D^{(\alpha)})|} + O(\delta). \end{aligned}$$

Combining this with (3.3) and (3.4) gives the result, provided that the $O(\delta)$ remainder term is well behaved as $\alpha, \epsilon \rightarrow 0$. Uniformity with respect to ϵ follows from ([33], theorem 2) and uniformity with respect to small values of α follows similarly. The crucial property is that theorem 2.9 gives an expansion of this form for any configuration of non-overlapping resonators. This is based on the asymptotic expansion (2.6) of $\mathcal{S}_D^k[\phi]$ as $k \rightarrow 0$, in which each term has the form $\mathcal{S}_{D,n}[\phi](x)$, for $n = 1, 2, \dots$, where

$$\mathcal{S}_{D,n}[\phi](x) = -\frac{i^n}{4\pi n!} \int_{\partial D} |x - y|^{n-1} \phi(y) \, d\sigma(y), \quad x \in \partial D. \quad (3.5)$$

The leading-order equation gives us that $\phi \in \text{span}\{\psi_1, \dots, \psi_N\}$, where $\psi_i = (\mathcal{S}_D^0)^{-1}[\chi_{\partial D_i}]$ (see [32], lemma 2.6 for details). If we rescale one of the domains $D_i \mapsto (1 + \alpha_i)D_i$, then the quantities $\mathcal{S}_{D,n}[\psi_i](x)$ depend continuously on α_i . Thus, if α is sufficiently small that the resonators do not overlap, then taking the supremum of these continuous quantities over $\alpha_i \in (-\alpha, \alpha)$ gives a bound that holds uniformly over all such (sufficiently small) values of α . ■

Remark 3.6. While the Wielandt–Hoffman theorem was used in (3.3), there are a range of results that could be invoked here. For example, if λ_{\min} and λ_{\max} are the smallest and largest eigenvalues of A , then it holds that

$$\lambda_n^\epsilon(D) + \lambda_{\min} \leq \lambda_i^\epsilon(D^{(\alpha)}) \leq \lambda_n^\epsilon(D) + \lambda_{\max},$$

for all $n = 1, \dots, N$. For a selection of results on perturbations of eigenvalues of symmetric matrices, see [34].

Theorem 3.5 shows that if a dilute array is deformed by changing the sizes of the resonators, then the induced change in the resonant frequencies is expected to be small. This is demonstrated numerically in figure 5, where we simulate the full differential system and can see that the changes in the frequencies are asymptotically small when the perturbations are small.

(c) Changes in position

Let us now consider imperfections due to changes in the positions of the resonators. In particular, suppose there exist some vectors $\beta_1, \dots, \beta_N \in \mathbb{R}^3$ such that the perturbed structure is given by

$$D^{(\beta)} = \bigcup_{i=1}^N (B_i + \epsilon^{-1}(z_i + \beta_i)). \quad (3.6)$$

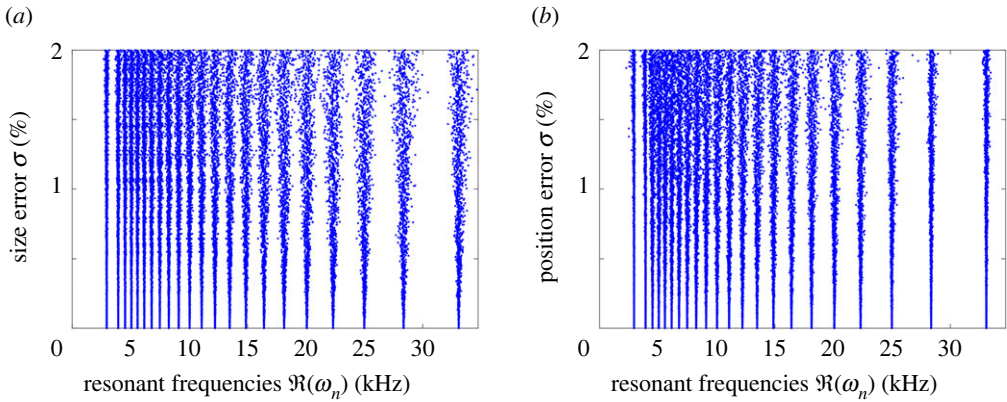


Figure 5. The effect of random errors and imperfections on the subwavelength resonant frequencies of a cochlea-inspired rainbow sensor. (a) Random errors are added to the sizes of the resonators. (b) Random errors are added to the positions of the resonators. In both cases the errors are Gaussian with mean zero and variance σ^2 . These simulations are performed on the full differential problem using the multipole expansion method. The deviation of the random error σ is expressed as a percentage of the unperturbed values.

We will assume that the perturbations β_1, \dots, β_N are small in the sense that there exists some parameter $\beta \in \mathbb{R}$ such that $\|\beta_i\| = O(\beta)$ as $\beta \rightarrow 0$. We will proceed as in the previous section, by considering the dilute generalized capacitance matrix C^ϵ .

Lemma 3.7. *Suppose that a resonator array D is deformed to give $D^{(\beta)}$, as defined in (3.6), and that the translation vectors β_1, \dots, β_N satisfy $\|\beta_i\| = O(\beta)$ as $\beta \rightarrow 0$ for all $i = 1, \dots, N$. Then, for fixed $0 < \epsilon \ll 1$, the dilute generalized capacitance matrix associated with $D^{(\beta)}$ is given by*

$$C^\epsilon(D^{(\beta)}) = C^\epsilon(D) + B(\beta),$$

where $B(\beta)$ is a symmetric $N \times N$ -matrix whose Frobenius norm satisfies $\|B\|_F = O(\beta)$ as $\beta \rightarrow 0$. Furthermore, the error bound $\|C^\epsilon(D^{(\beta)}) - C^\epsilon(D)\|_F = O(\beta)$ as $\beta \rightarrow 0$ is uniform with respect to $\epsilon \in [0, 1]$.

Proof. We will make the substitution $z_i \mapsto z_i + \beta_i$ in definition 3.1. The diagonal entries of C^ϵ are unchanged. For the off-diagonal entries, we have that

$$C_{ij}^\epsilon(D^{(\beta)}) = -\epsilon \frac{\text{Cap}_{B_i} \text{Cap}_{B_j}}{4\pi |z_i + \beta_i - z_j - \beta_j| \sqrt{|B_i| |B_j|}}, \quad i \neq j.$$

For small β we can expand the denominator to give

$$\frac{1}{|z_i + \beta_i - z_j - \beta_j|} = \frac{1}{|z_i - z_j|} - (\beta_i - \beta_j) \cdot \frac{z_i - z_j}{|z_i - z_j|^3} + O(\beta^2), \quad i \neq j,$$

as $\beta \rightarrow 0$. This gives us that

$$C_{ij}^\epsilon(D^{(\beta)}) = C_{ij}^\epsilon(D) + \epsilon(\beta_i - \beta_j) \cdot \frac{(z_i - z_j) \text{Cap}_{B_i} \text{Cap}_{B_j}}{4\pi |z_i - z_j|^3 \sqrt{|B_i| |B_j|}} + O(\beta^2), \quad i \neq j, \quad (3.7)$$

as $\beta \rightarrow 0$. The uniformity follows by taking the supremum of (3.7) with respect to $\epsilon \in [0, 1]$. ■

Theorem 3.8. *Suppose that a resonator array D is ϵ -dilute in the sense of (3.1) and is deformed to give $D^{(\beta)}$, as defined in (3.6), for translation vectors β_1, \dots, β_N which satisfy $\|\beta_i\| = O(\beta)$ as $\beta \rightarrow 0$ for all*

$i = 1, \dots, N$. Then the resonant frequencies satisfy

$$|\omega_n(D) - \omega_n(D^{(\beta)})| = O\left(\sqrt{\delta(\beta + \epsilon^2)}\right),$$

as $\beta, \delta, \epsilon \rightarrow 0$.

Proof. From lemma 3.7, we have that $C^\epsilon(D^{(\beta)}) = C^\epsilon(D) + B(\beta)$ where B is a symmetric $N \times N$ -matrix so we can proceed as in theorem 3.5 to use the Wielandt–Hoffman theorem to bound $|\lambda_n^\epsilon(D) - \lambda_n^\epsilon(D^{(\beta)})|$ by $\|B\|_F$ for each $n = 1, \dots, N$. Then, approximating under the assumption that δ and ϵ are small gives the result. ■

Theorem 3.8 is the analogue of theorem 3.5 and bounds the changes in the resonant frequencies when the positions of the resonators are changed. This is again demonstrated numerically in figure 5.

(d) Higher-order results

Recall the expansion $\omega_n = \sqrt{\delta v^2 \lambda_n} - i\delta\tau_n + \dots$ from theorem 2.9. The formula for τ_n involves the eigenvectors \mathbf{v}_n of the generalized capacitance matrix. Assuming the material parameters are real, τ_n describes the leading-order imaginary part of the resonant frequency, so it is important to understand how it is affected by imperfections in the structure.

If we consider a resonator array D that is such that the associated (symmetric) generalized capacitance matrix $\mathcal{C}(D)$ has N distinct, simple eigenvalues, then we can derive an approximate formula for the effects of perturbations on the eigenvectors of $\mathcal{C}(D)$. Suppose that a perturbation, governed by the parameter γ , is made to the structure to give $D^{(\gamma)}$ and that there is a symmetric matrix $\Gamma(\gamma)$ which is such that

$$\mathcal{C}(D^{(\gamma)}) = \mathcal{C}(D) + \Gamma(\gamma), \quad (3.8)$$

where $\|\Gamma(\gamma)\| \rightarrow 0$ as $\gamma \rightarrow 0$. In this setting, we can derive an approximate formula for the perturbed eigenvector $\mathbf{v}_n(D^{(\gamma)})$.

Since $\mathcal{C}(D)$ is a symmetric matrix, it has an orthonormal basis of eigenvectors $\{\mathbf{v}_n : n = 1, \dots, N\}$ with associated eigenvalues $\sigma(\mathcal{C}(D)) = \{\lambda_n : n = 1, \dots, N\}$, which are assumed to be distinct. Under this assumption, we have the decomposition

$$(\lambda I - \mathcal{C}(D))^{-1}x = \sum_{k=1}^N \frac{\langle x, \mathbf{v}_k \rangle}{\lambda - \lambda_k} \mathbf{v}_k, \quad x \in \mathbb{C}^n, \lambda \in \mathbb{C} \setminus \sigma(\mathcal{C}). \quad (3.9)$$

From this, we can see that $\|(\lambda I - \mathcal{C}(D))^{-1}\| \leq \text{dist}(\lambda, \sigma(\mathcal{C}(D)))^{-1}$. If we add a perturbation matrix $\Gamma(\gamma)$ which is such that $\|\Gamma(\gamma)\| < \text{dist}(\lambda, \sigma(\mathcal{C}(D)))$, then $\lambda I - \mathcal{C}(D^{(\gamma)}) = \lambda I - \mathcal{C}(D) - \Gamma(\gamma)$ is invertible. Further, in this case, we can use a Neumann series to see that

$$(\lambda I - \mathcal{C}(D^{(\gamma)}))^{-1} = (\lambda I - \mathcal{C}(D) - \Gamma)^{-1} = (\lambda I - \mathcal{C}(D))^{-1} \sum_{i=0}^{\infty} \Gamma^i ((\lambda I - \mathcal{C}(D))^{-1})^i. \quad (3.10)$$

Substituting the decomposition (3.9) and taking only the first two terms from (3.10), we see that for a fixed $\lambda \in \mathbb{C} \setminus \sigma(\mathcal{C})$ we have

$$(\lambda I - \mathcal{C}(D^{(\gamma)}))^{-1} = \sum_{k=1}^N \frac{\langle \cdot, \mathbf{v}_k \rangle}{\lambda - \lambda_k} \mathbf{v}_k + \sum_{k=1}^N \sum_{j=1}^N \frac{\langle \cdot, \mathbf{v}_j \rangle \langle \Gamma \mathbf{v}_j, \mathbf{v}_k \rangle}{(\lambda - \lambda_k)(\lambda - \lambda_j)} \mathbf{v}_k + \dots, \quad (3.11)$$

where the remainder terms are $O(\|\Gamma(\gamma)\|^2)$ as $\gamma \rightarrow 0$.

Suppose we have a collection of closed curves $\{\eta_n : n = 1, \dots, N\}$ which do not intersect and are such that the interior of each curve η_n contains exactly one eigenvalue λ_n . We know that we may choose γ to be sufficiently small that the eigenvalues of $\mathcal{C}(D^{(\gamma)})$ remain within the interior of these

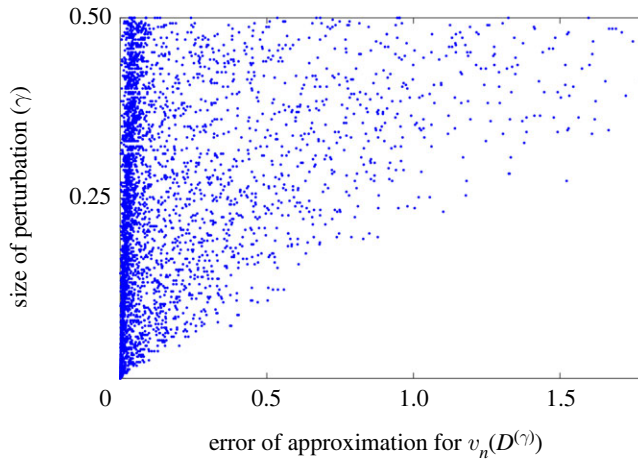


Figure 6. The error of the approximation for $\mathbf{v}_n(D^{(\gamma)})$ derived in (3.13) is small for small perturbations γ , which are expressed as percentages of the unperturbed values. We repeatedly simulate randomly perturbed cochlea-inspired rainbow sensors and compare the exact value with the approximate value from (3.13).

same curves. Thus, the operator $P_n : \mathbb{C}^N \rightarrow \mathbb{C}^N$, defined by

$$P_n = \frac{1}{2\pi i} \int_{\eta_n} (\lambda I - C(D^{(\gamma)}))^{-1} d\lambda, \quad (3.12)$$

is the projection onto the eigenspace associated with the perturbed eigenvalue $\lambda_n(D^{(\gamma)})$. Using the expansion (3.11), we can calculate an approximation to the operator P_n , given by

$$P_n \approx \langle \cdot, \mathbf{v}_n \rangle \mathbf{v}_n + \sum_{\substack{k=1 \\ k \neq n}}^N \frac{\langle \cdot, \mathbf{v}_n \rangle \langle \Gamma \mathbf{v}_n, \mathbf{v}_k \rangle}{(\lambda_n - \lambda_k)} \mathbf{v}_k,$$

where we are assuming the remainder term to be small in order for the approximation to hold. This is a technical issue, which is not trivial to show precisely due to the non-uniformity of the expansion (3.11) with respect to λ , particularly near to $\lambda \in \sigma(\mathcal{C}(D))$. Applying this approximation for the operator P_n to the unperturbed eigenvector \mathbf{v}_n gives the desired approximation

$$\mathbf{v}_n(D^{(\gamma)}) \approx \mathbf{v}_n(D) + \sum_{\substack{k=1 \\ k \neq n}}^N \frac{\langle \Gamma(\gamma) \mathbf{v}_n(D), \mathbf{v}_k(D) \rangle}{(\lambda_n - \lambda_k)} \mathbf{v}_k(D), \quad (3.13)$$

provided that γ is sufficiently small.

The formula in (3.13) is approximate in the sense that we do not have estimates for the error and, instead, we have *assumed* the remainder term is uniformly small in the underlying asymptotic expansion. However, we can verify the accuracy of this formula through simulations, presented in figure 6, where we compare the approximate eigenvector from (3.13) and the true eigenvector for many randomly perturbed cochlea-inspired rainbow sensors. We see that the errors are small when the size of the perturbations γ is small.

4. Removing resonators from the device

We will now consider a different class of perturbations of the rainbow sensors: the effect of removing a resonator from the array. This is shown in figure 7. This is inspired by observations of the biological cochlea where in many places the receptor cells are so badly damaged that the stereocilia have been completely destroyed, as depicted in figure 1.

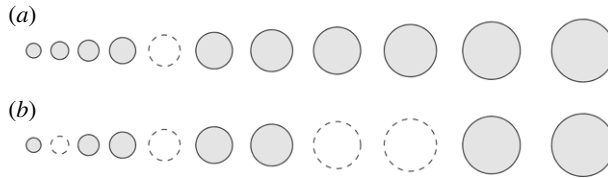


Figure 7. We study the effects of removing resonators from a cochlea-inspired rainbow sensor. (a) The rainbow sensor with a single resonator removed, denoted $D^{(5)}$. (b) The rainbow sensor with multiple resonators removed, denoted $D^{(2,5,8,9)}$. The original rainbow sensor, $D = D_1 \cup \dots \cup D_{11}$, is shown in dashes.

We introduce some notation to describe a system of resonators with one or more resonators removed. Given a resonator array D we write $D^{(i)}$ to denote the same array with the i th resonator removed. The resonators are labelled according to increasing volume (so, from left to right in the graded cochlea-inspired rainbow sensors depicted here, as in figure 2). For the removal of multiple resonators, we add additional subscripts. For example, in figure 7a we show $D^{(5)} = D_1 \cup \dots \cup D_4 \cup D_6 \cup \dots \cup D_{11}$ and in figure 7b we show $D^{(2,5,8,9)}$, which has the 2nd, 5th, 8th and 9th resonators removed.

The crucial result that underpins the analysis in this section is Cauchy's Interlacing Theorem, which describes the relation between a Hermitian matrix's eigenvalues and the eigenvalues of its principal submatrices. A principle submatrix is a matrix obtained by removing rows and columns (with the same indices) from a matrix.

Theorem 4.1 (Cauchy's Interlacing Theorem). *Let A be an $N \times N$ Hermitian matrix with eigenvalues $\lambda_1 \leq \lambda_2 \leq \dots \leq \lambda_N$. Suppose that B is an $(N - 1) \times (N - 1)$ principal submatrix of A with eigenvalues $\mu_1 \leq \mu_2 \leq \dots \leq \mu_{N-1}$. Then, the eigenvalues are ordered such that $\lambda_1 \leq \mu_1 \leq \lambda_2 \leq \mu_2 \leq \dots \leq \lambda_{N-1} \leq \mu_{N-1} \leq \lambda_N$.*

Proof. Various proof strategies exist, see [34] or [35], for example. ■

Thanks to Cauchy's Interlacing Theorem, we can quickly obtain a result for the eigenvalues of the generalized capacitance matrix. In order to state a result for the resonant frequencies of a resonator array, we will first introduce some asymptotic notation.

Definition 4.2. For non-negative real-valued functions f and g , we will write that $f(\delta) \gtrsim g(\delta)$ as $\delta \rightarrow 0$ if

$$\lim_{\delta \rightarrow 0} \frac{f(\delta)}{\max\{f(\delta), g(\delta)\}} = 1, \quad \text{as } \delta \rightarrow 0,$$

where we define the ratio to be 1 in the event that $0 = f = g$.

Lemma 4.3. *Let D be a resonator array and $D^{(i)}$ be the same array with the i th resonator removed. Then, if δ is sufficiently small, the resonant frequencies of the two structures interlace in the sense that*

$$\Re(\omega_j(D)) \lesssim \Re(\omega_j(D^{(i)})) \lesssim \Re(\omega_{j+1}(D)) \quad \text{for all } j = 1, \dots, N - 1.$$

Proof. Since $\mathcal{C}(D)$ is symmetric and real valued, we can use Cauchy's Interlacing Theorem (theorem 4.1) to see that

$$\lambda_j(D) \leq \lambda_j(D^{(i)}) \leq \lambda_{j+1}(D) \quad \text{for all } j = 1, \dots, N - 1.$$

Then, the result follows from the asymptotic formula in theorem 2.9. ■

The subwavelength resonant frequencies of resonator arrays with an increasing number of removed resonators are shown in figure 8. We see that the frequencies interlace those of the previous structure and remain distributed across the audible range. In general, we observe that removing resonators at different parts of the array affects different parts of the spectrum more strongly. If the larger resonators are removed, then the lower frequencies in the spectrum

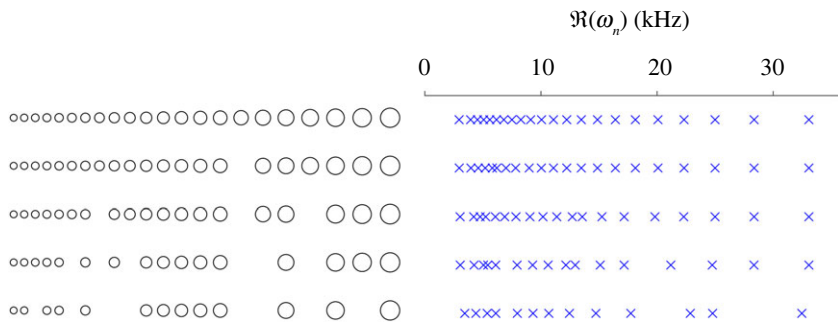


Figure 8. The subwavelength resonant frequencies of a cochlea-inspired rainbow sensor with resonators removed. Each subsequent array has additional resonators removed and its set of resonant frequencies interlaces the previous, at leading order, as predicted by lemma 4.3.

experience the strongest perturbations, while removing the smallest resonators affects the highest frequencies more significantly. This matches the intuition gained from the resonant frequencies of the uncoupled resonators and, crucially, all takes place within the bounds posed by the interlacing property from lemma 4.3.

(a) Stable removal from large devices

In general, lemma 4.3 is useful for understanding the effect of removing a resonator but does not give stability, in the sense of the perturbation being small. However, a cochlea-inspired rainbow sensor with a large number of resonators can be designed such that the resonant frequencies are bounded, even as their number becomes very large. In this case, many of the gaps between the real parts will be small and, subsequently, so will the perturbations caused by removing a resonator. There are a variety of ways to formulate this precisely, one version is given in the following theorem.

Theorem 4.4. *Suppose that a resonator array D is dilute with parameter $0 < \epsilon \ll 1$ in the sense that*

$$D = \bigcup_{j=1}^N (B + \epsilon^{-1}z_j),$$

where B is a fixed bounded domain and $\epsilon^{-1}z_j$ represents the position of each resonator. Then, there exists a constant $c \in \mathbb{R}$, which does not depend on N or ϵ , such that if $\epsilon = c/N$, then all the eigenvalues $\{\lambda_j\}$ of C^ϵ are such that

$$0 < \lambda_j < \frac{2|\text{Cap}_B|}{|B|}. \tag{4.1}$$

Proof. In this case, the dilute generalized capacitance matrix is given by

$$C_{ij}^\epsilon = \begin{cases} \frac{\text{Cap}_B}{|B|}, & i = j, \\ -\frac{\epsilon \text{Cap}_B^2}{4\pi |B| |z_i - z_j|}, & i \neq j. \end{cases} \tag{4.2}$$

By the Gershgorin circle theorem, we know that the eigenvalues $\{\lambda_j : j = 1, \dots, N\}$ must be such that

$$\left| \lambda_j - \frac{\text{Cap}_B}{|B|} \right| \leq \frac{\epsilon \text{Cap}_B^2}{4\pi |B|} \sum_{i \neq j} \frac{1}{|z_i - z_j|}, \quad j = 1, \dots, N. \tag{4.3}$$

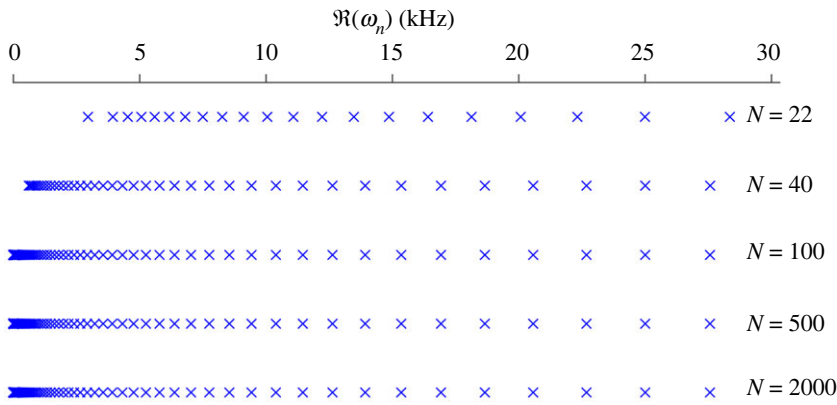


Figure 9. Large cochlea-inspired rainbow sensors can be designed such that the subwavelength resonant frequencies are bounded. Here, we simulate successively larger arrays using the multipole expansion to solve the full differential problem, with the configuration of the resonators being chosen according to the dilute regime defined in theorem 4.4.

Now, we have that

$$\frac{\epsilon \text{Cap}_B}{4\pi} \sum_{i \neq j} \frac{1}{|z_i - z_j|} \leq \epsilon(N - 1) \frac{\text{Cap}_B}{4\pi} \sup_{i \neq j} |z_i - z_j|^{-1},$$

which we can choose to be less than 1 by selecting $c = \epsilon N$ appropriately. In which case, we have that the eigenvalues $\{\lambda_j : j = 1, \dots, N\}$ satisfy

$$\left| \lambda_j - \frac{\text{Cap}_B}{|B|} \right| \leq \frac{\text{Cap}_B}{|B|}, \quad j = 1, \dots, N.$$

■

It is important to note that theorem 4.4 merely shows that the real parts of the resonant frequencies will be bounded, as the number of resonators becomes large. It does not guarantee that they are evenly spaced or that the gaps between any particular adjacent resonant frequencies are small. For example, see figure 9, where the subwavelength resonant frequencies for increasingly large arrays, dimensioned according to theorem 4.4, are shown. We see that the frequencies become very dense in part of the range but remain sparser at higher frequencies.

5. Implications for signal processing

The aim of the cochlea-like rainbow sensor studied in this work is to replicate the ability of the cochlea to filter sounds. There is also a large community of researchers developing signal processing algorithms with the same aim: to replicate the abilities of the human auditory system. Since we have precise analytic methods to describe how the array scatters an incoming field, we can draw comparisons between the cochlea-inspired rainbow sensor studied here and biomimetic signal transforms. This is explored in detail in [12]. In particular, given a formula for the field that is scattered by the cochlea-inspired rainbow sensor, we can deduce the corresponding signal transform. In this section, we explore how this signal transform is affected by the introduction of errors and imperfections.

(a) A biomimetic signal transform

We briefly recall from [12] how a biomimetic signal transform can be deduced from a cochlea-inspired rainbow sensor. In response to an incoming wave u^{in} , the solution to the Helmholtz

problem (2.3) is given, for $x \in \mathbb{R}^3 \setminus \bar{D}$, as

$$u(x) - u^{\text{in}}(x) = \sum_{n=1}^N q_n \mathcal{S}_D^k[\psi_n](x) - \mathcal{S}_D^{k_0}[\mathcal{S}_D^{-1}[u^{\text{in}}]](x) + O(\omega), \quad (5.1)$$

as $\omega \rightarrow 0$, where $\psi_n = (\mathcal{S}_D^0)^{-1}[\chi_{\partial D_n}]$ and the constants q_n satisfy

$$(\omega^2 I - v_b^2 \delta \mathcal{C}) \begin{pmatrix} q_1 \\ \vdots \\ q_N \end{pmatrix} = v_b^2 \delta \begin{pmatrix} \frac{1}{|D_1|} \int_{\partial D_1} \mathcal{S}_D^{-1}[u^{\text{in}}] d\sigma \\ \vdots \\ \frac{1}{|D_N|} \int_{\partial D_N} \mathcal{S}_D^{-1}[u^{\text{in}}] d\sigma \end{pmatrix} + O(\delta\omega + \omega^3), \quad (5.2)$$

as $\omega, \delta \rightarrow 0$. Suppose that the incoming wave is a plane wave and can be written in terms of some real-valued function s as

$$u^{\text{in}}(x, \omega) = \int_{-\infty}^{\infty} s\left(\frac{x_1}{v-t}\right) e^{i\omega t} dt. \quad (5.3)$$

Assuming that we are in an appropriate low-frequency regime, such that the remainder terms remain small, we can apply a Fourier transform to (5.1) to see that the scattered pressure field $p(x, t)$ is given by

$$p(x, t) = \sum_{n=1}^N a_n[s](t) u_n(x) + \dots,$$

where the remainder term is $O(\delta)$ and the coefficients are given by

$$a_n[s](t) = (s * h[\omega_n])(t), \quad n = 1, \dots, N, \quad (5.4)$$

for kernels defined as

$$h[\omega_n](t) = \begin{cases} 0, & t < 0, \\ c_n e^{\Im(\omega_n)t} \sin(\Re(\omega_n)t), & t \geq 0, \end{cases} \quad n = 1, \dots, N, \quad (5.5)$$

for some real-valued constants c_n . Recall that $\Im(\omega_n) < 0$ due to energy loss, so $h[\omega_n](t)$ decays as $t \rightarrow \infty$. See [12] for details of this derivation, which relies on computing the integrals resulting from applying a Fourier transform to (5.1), performed by using the residue theorem to calculate the contributions from the poles at each resonant frequency (in the lower complex plane). Thus, the deduced signal transform is: given a signal s , compute the N time-varying outputs $a_n[s]$, defined by (5.4).

(b) Stability to errors

We wish to show that the signal transform $s \mapsto a_n[s] := s * h[\omega_n]$ is robust with respect to errors and imperfections in the design of the underlying cochlea-inspired rainbow sensor.

Theorem 5.1. *Given two complex numbers ω^{old} and ω^{new} with negative imaginary parts, it holds that*

$$\|s * h[\omega^{\text{old}}] - s * h[\omega^{\text{new}}]\|_{L^\infty(\mathbb{R})} \leq \|h[\omega^{\text{old}}] - h[\omega^{\text{new}}]\|_{L^\infty(\mathbb{R})} \|s\|_{L^1(\mathbb{R})},$$

for all $s \in L^1(\mathbb{R})$.

Proof. This is a standard argument for bounding convolutions:

$$\begin{aligned} \|s * h[\omega^{\text{old}}] - s * h[\omega^{\text{new}}]\|_{L^\infty(\mathbb{R})} &\leq \sup_{x \in \mathbb{R}} \int_{\mathbb{R}} |s(x-y)| |h[\omega^{\text{old}}](y) - h[\omega^{\text{new}}](y)| dy \\ &\leq \|h_n^{\text{old}} - h_n^{\text{new}}\|_{L^\infty(\mathbb{R})} \sup_{x \in \mathbb{R}} \int_{\mathbb{R}} |s(x-y)| dy \\ &= \|h_n^{\text{old}} - h_n^{\text{new}}\|_{L^\infty(\mathbb{R})} \|s\|_{L^1(\mathbb{R})}. \end{aligned}$$



Remark 5.2. If s is compactly supported, then we can reframe theorem 5.1 in terms of $\|\cdot\|_{L^p(\mathbb{R})}$ for any $1 \leq p \leq \infty$, using Hölder's inequality.

Corollary 5.3. Let $c > 0$ and suppose we have two complex numbers ω^{old} and ω^{new} whose imaginary parts satisfy $\Im(\omega^{old}), \Im(\omega^{new}) \leq -c$. Then, it holds that

$$\|s * h[\omega^{old}] - s * h[\omega^{new}]\|_{L^\infty(\mathbb{R})} \leq \frac{\sqrt{2}}{ce} |\omega^{old} - \omega^{new}| \|s\|_{L^1(\mathbb{R})},$$

for all $s \in L^1(\mathbb{R})$.

Proof. We begin with the observation that

$$\begin{aligned} & |h[\omega^{old}](t) - h[\omega^{new}](t)| \\ &= |(e^{\Im(\omega^{old})t} - e^{\Im(\omega^{new})t}) \sin(\Re(\omega^{old})t) + e^{\Im(\omega^{new})t} (\sin(\Re(\omega^{old})t) - \sin(\Re(\omega^{new})t))|, \end{aligned}$$

for $t > 0$. Then, we have that

$$|(e^{\Im(\omega^{old})t} - e^{\Im(\omega^{new})t}) \sin(\Re(\omega^{old})t)| \leq |e^{\Im(\omega^{old})t} - e^{\Im(\omega^{new})t}| \leq \frac{1}{ce} |\Im(\omega^{old}) - \Im(\omega^{new})|,$$

for $t > 0$, where we have used the fact that $\sup_{t>0} \sup_{\omega < -c} |t e^{\omega t}| = 1/ce$. Similarly, we have that

$$|e^{\Im(\omega^{new})t} (\sin(\Re(\omega^{old})t) - \sin(\Re(\omega^{new})t))| \leq \frac{1}{ce} |\Re(\omega^{old}) - \Re(\omega^{new})|$$

for $t > 0$, where we have used the fact that $\sup_{t>0} \sup_{\omega < -c} |t e^{\omega t} \cos(at)| \leq 1/ce$ for any $a \in \mathbb{R}$. Putting this together, we have that

$$\|s * h[\omega^{old}] - s * h[\omega^{new}]\|_{L^\infty(\mathbb{R})} \leq \frac{1}{ce} (|\Im(\omega^{old}) - \Im(\omega^{new})| + |\Re(\omega^{old}) - \Re(\omega^{new})|) \|s\|_{L^1(\mathbb{R})},$$

from which we arrive at the result, using the inequality $|a| + |b| \leq \sqrt{2(a^2 + b^2)}$. ■

While theorem 5.1 is the standard stability result for convolutional signal processing algorithms, corollary 5.3 is most revealing here. It shows that the outputs of the induced biomimetic signal transform (defined by (5.4) here) are stable with respect to changes in the resonant frequencies of the physical device. From §§3 and 4, we know that the resonant frequencies of the cochlea-inspired rainbow sensor are robust with respect to a variety of errors and imperfections (particularly in large dilute resonator arrays), meaning that the biomimetic signal transform inherits this robustness.

To test the robustness for small arrays with removed resonators, figure 10 shows the frequency support of the filter array used in the biomimetic signal transform in the case of successively removed resonators (the same sequence of structures was simulated in figure 8). In this small array (of 22 resonators, initially), we see that gaps emerge when multiple resonators are removed, corresponding to hearing loss at frequencies within these gaps. We observe that even when a significant proportion of resonators are removed from the array, the support of the filter array still covers a large proportion of the range of audible frequencies.

6. Conclusion

The formulae derived in this work show that a cochlea-inspired rainbow sensor is robust with respect to small perturbations in the position and size of the constituent resonators. The effect of removing resonators was also described; it was shown that the change in the subwavelength resonant frequencies can always be bounded via an interlacing theorem and that the resulting change in the spectrum can be small in the case of sufficiently large, dilute arrays. The implications of this analysis for related biomimetic signal transforms were also studied, and it was shown that stability properties are inherited from the underlying resonant frequencies.

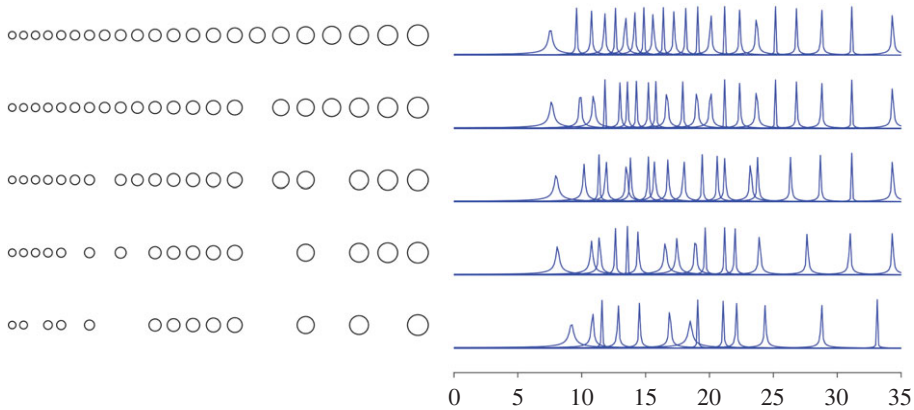


Figure 10. The frequency supports of the filter kernels $h[\omega_n]$ induced by a cochlea-inspired rainbow sensor. Each subsequent array has additional resonators removed and for each array, we plot the Fourier transform of $h[\omega_n]$, $n = 1, \dots, N$, normalized in $L^2(\mathbb{R})$.

The analysis in this work suggests possible mechanisms through which sufficiently large structures could be robust to (surprisingly) large perturbations. However, the extent to which this truly replicates the remarkable robustness of the cochlea is unclear. While the mechanisms which underpin the function of cochlea-inspired rainbow sensors (which are locally resonant graded metamaterials) and biological cochleae (which have a graded membrane with receptor cells on the surface) are quite different, there is scope for further insight to be traded between the two communities. For example, there has recently been new insight into the role of topological protection in rainbow sensors [21] and in signal processing devices [36]. Conversely, we observed a tendency for gaps in the frequency support of the filter array to appear more commonly at higher frequencies (see figure 10, for example). This is (qualitatively) consistent with the observation that human hearing loss initially occurs at high frequencies in most people [23]. It is not yet clear if either of these ideas can be transposed between the two realms of biological hearing models and cochlea-inspired devices.

Data accessibility. The code used in this study is available at <https://doi.org/10.5281/zenodo.5541152>.

Authors' contributions. B.D.: conceptualization, formal analysis, investigation, methodology, project administration, resources, software, supervision, validation, visualization, writing—review and editing. L.H.: formal analysis, investigation, software, validation, visualization, writing—original draft, writing—review and editing.

All authors gave final approval for publication and agreed to be held accountable for the work performed therein.

Conflict of interest declaration. We declare we have no competing interests.

Funding. The work of B.D. was supported by the European Commission H2020 FETOpen project BOHEME under grant agreement no. 863179.

Acknowledgements. The authors would like to thank Habib Ammari for his insightful suggestions and Elizabeth M. Keithley for providing the micrographs in figure 1. The comments and suggestions of anonymous reviewers were valuable in improving the presentation of this article.

References

1. Rupin M, Lerosey G, de Rosny J, Lemoult F. 2019 Mimicking the cochlea with an active acoustic metamaterial. *New J. Phys.* **21**, 093012. (doi:10.1088/1367-2630/ab3d8f)
2. Ammari H, Davies B. 2020 Mimicking the active cochlea with a fluid-coupled array of subwavelength Hopf resonators. *Proc. R. Soc. A* **476**, 20190870. (doi:10.1098/rspa.2019.0870)
3. Karlos A, Elliott SJ. 2020 Cochlea-inspired design of an acoustic rainbow sensor with a smoothly varying frequency response. *Sci. Rep.* **10**, 1–11. (doi:10.1038/s41598-020-67608-z)

4. Ammari H, Davies B. 2019 A fully coupled subwavelength resonance approach to filtering auditory signals. *Proc. R. Soc. A* **475**, 20190049. (doi:10.1098/rspa.2019.0049)
5. Babbs CF. 2011 Quantitative reappraisal of the Helmholtz-Guyton resonance theory of frequency tuning in the cochlea. *J. Biophys.* **2011**, 1–16. (doi:10.1155/2011/435135)
6. Zhao L, Zhou S. 2019 Compact acoustic rainbow trapping in a bioinspired spiral array of graded locally resonant metamaterials. *Sensors* **19**, 788. (doi:10.3390/s19040788)
7. Zhu J, Chen Y, Zhu X, Garcia-Vidal FJ, Yin X, Zhang W, Zhang X. 2013 Acoustic rainbow trapping. *Sci. Rep.* **3**, 1728. (doi:10.1038/srep01728)
8. Tsakmakidis KL, Boardman AD, Hess O. 2007 ‘Trapped rainbow’ storage of light in metamaterials. *Nature* **450**, 397–401. (doi:10.1038/nature06285)
9. Bennetts LG, Peter MA, Craster RV. 2018 Graded resonator arrays for spatial frequency separation and amplification of water waves. *J. Fluid Mech.* **854**, R4. (doi:10.1017/jfm.2018.648)
10. Jang MS, Atwater H. 2011 Plasmonic rainbow trapping structures for light localization and spectrum splitting. *Phys. Rev. Lett.* **107**, 207401. (doi:10.1103/PhysRevLett.107.207401)
11. Joyce BS, Tarazaga PA. 2015 Developing an active artificial hair cell using nonlinear feedback control. *Smart Mater. Struct.* **24**, 094004. (doi:10.1088/0964-1726/24/9/094004)
12. Ammari H, Davies B. 2020 Asymptotic links between signal processing, acoustic metamaterials and biology. (<http://arxiv.org/abs/2005.12794>).
13. Lyon RF. 2017 *Human and machine hearing*. Cambridge, UK: Cambridge University Press.
14. Hughes TW, Williamson IA, Minkov M, Fan S. 2019 Wave physics as an analog recurrent neural network. *Sci. Adv.* **5**, eaay6946. (doi:10.1126/sciadv.aay6946)
15. Hudspeth A. 2008 Making an effort to listen: mechanical amplification in the ear. *Neuron* **59**, 530–545. (doi:10.1016/j.neuron.2008.07.012)
16. Craster RV, Guenneau S. 2013 *Acoustic metamaterials: negative refraction, imaging, lensing and cloaking*, vol. 166. Springer Series in Materials Science. London, UK: Springer.
17. Kadic M, Milton GW, van Hecke M, Wegener M. 2019 3D metamaterials. *Nat. Rev. Phys.* **1**, 198–210. (doi:10.1038/s42254-018-0018-y)
18. Khanikaev AB, Mousavi SH, Tse WK, Kargarian M, MacDonald AH, Shvets G. 2013 Photonic topological insulators. *Nat. Mater.* **12**, 233–239. (doi:10.1038/nmat3520)
19. Fefferman CL, Lee-Thorp JP, Weinstein MI. 2017 Topologically protected states in one-dimensional systems. In *Memoirs of the American Mathematical Society*, vol. 247. Providence, RI: AMS.
20. Ammari H, Davies B, Hiltunen EO, Yu S. 2020 Topologically protected edge modes in one-dimensional chains of subwavelength resonators. *J. Math. Pures Appl.* **144**, 17–49. (doi:10.1016/j.matpur.2020.08.007)
21. Chaplain GJ, De Ponti JM, Aguzzi G, Colombi A, Craster RV. 2020 Topological rainbow trapping for elastic energy harvesting in graded Su-Schrieffer-Heeger systems. *Phys. Rev. Appl.* **14**, 054035. (doi:10.1103/PhysRevApplied.14.054035)
22. Centres for Disease Control and Prevention, US. Department of Health & Human Services. 2020 How Does Loud Noise Cause Hearing Loss?. See https://www.cdc.gov/nceh/hearing_loss/how_does_loud_noise_cause_hearing_loss.html (accessed on 24 September 2021).
23. Wu P, O’Malley JT, de Gruttola V, Liberman MC. 2020 Age-related hearing loss is dominated by damage to inner ear sensory cells, not the cellular battery that powers them. *J. Neurosci.* **40**, 6357–6366. (doi:10.1523/JNEUROSCI.0937-20.2020)
24. Minnaert M. 1933 On musical air-bubbles and the sounds of running water. *Philos. Mag.* **16**, 235–248. (doi:10.1080/14786443309462277)
25. Devaud M, Hocquet T, Bacri JC, Leroy V. 2008 The Minnaert bubble: an acoustic approach. *Eur. J. Phys.* **29**, 1263. (doi:10.1088/0143-0807/29/6/014)
26. Ammari H, Fitzpatrick B, Gontier D, Lee H, Zhang H. 2018 Minnaert resonances for acoustic waves in bubbly media. *Ann. Inst. H. Poincaré Anal. Non Linéaire* **35**, 1975–1998. (doi:10.1016/j.anihpc.2018.03.007)
27. Leroy V, Bretagne A, Fink M, Willaime H, Tabelaing P, Tourin A. 2009 Design and characterization of bubble phononic crystals. *Appl. Phys. Lett.* **95**, 171904. (doi:10.1063/1.3254243)
28. Leroy V, Strybulevych A, Scanlon M, Page J. 2009 Transmission of ultrasound through a single layer of bubbles. *Eur. Phys. J. E* **29**, 123–130. (doi:10.1140/epje/i2009-10457-y)
29. Ammari H, Fitzpatrick B, Kang H, Ruiz M, Yu S, Zhang H. 2018 *Mathematical and computational methods in photonics and phononics*, vol. 235. Mathematical surveys and monographs. Providence, RI: American Mathematical Society.

30. Ammari H, Davies B, Hiltunen EO. 2021 Functional analytic methods for discrete approximations of subwavelength resonator systems. (<http://arxiv.org/abs/2106.12301>).
31. Diaz RA, Herrera WJ. 2011 The positivity and other properties of the matrix of capacitance: Physical and mathematical implications. *J. Electrostat.* **69**, 587–595. (doi:10.1016/j.elstat.2011.08.001)
32. Ammari H, Davies B, Hiltunen EO, Lee H, Yu S. 2022 *Wave interaction with subwavelength resonators*. Lecture Notes in Mathematics, C.I.M.E. Foundation Subseries. Berlin, Germany: Springer. (<https://arxiv.org/abs/2011.03575>)
33. Ammari H, Davies B, Hiltunen EO, Lee H, Yu S. 2021 High-order exceptional points and enhanced sensing in subwavelength resonator arrays. *Stud. Appl. Math.* **146**, 440–462. (doi:10.1111/sapm.12349)
34. Golub GH, Van Loan CF. 1983 *Matrix computations*, 3rd edn. Baltimore, MD: Johns Hopkins University Press.
35. Hwang SG. 2004 Cauchy's interlace theorem for eigenvalues of Hermitian matrices. *Am. Math. Monthly* **111**, 157–159. (doi:10.1080/00029890.2004.11920060)
36. Zangeneh-Nejad F, Fleury R. 2019 Topological analog signal processing. *Nat. Commun.* **10**, 1–10. (doi:10.1038/s41467-019-10086-3)